



Source Parameters of Moderate-To-Large Chinese Earthquakes From the Time Evolution of P-Wave Peak Displacement on Strong Motion Recordings

Yuan Wang^{1*}, Simona Colombelli², Aldo Zollo², Jindong Song¹ and Shanyou Li^{1*}

¹Key Laboratory of Earthquake Engineering and Engineering Vibration of China Earthquake Administration, Institute of Engineering Mechanics, China Earthquake Administration, Harbin, China, ²Department of Physics, University of Naples Federico II, Naples, Italy

OPEN ACCESS

Edited by:

Carmine Galasso,
University College London,
United Kingdom

Reviewed by:

Gemma Cremen,
University College London,
United Kingdom
Alon Ziv,
Tel Aviv University, Israel

*Correspondence:

Yuan Wang
wangyuanseis@gmail.com
Shanyou Li
shanyou@iem.ac.cn

Specialty section:

This article was submitted to
Geohazards and Georisks,
a section of the journal
Frontiers in Earth Science

Received: 11 October 2020

Accepted: 10 February 2021

Published: 18 March 2021

Citation:

Wang Y, Colombelli S, Zollo A, Song J and Li S (2021) Source Parameters of Moderate-To-Large Chinese Earthquakes From the Time Evolution of P-Wave Peak Displacement on Strong Motion Recordings. *Front. Earth Sci.* 9:616229. doi: 10.3389/feart.2021.616229

In this work we propose and apply a straightforward methodology for the automatic characterization of the extended earthquake source, based on the progressive measurement of the P-wave displacement amplitude at the available stations deployed around the source. Specifically, we averaged the P-wave peak displacement measurements among all the available stations and corrected the observed amplitude for distance attenuation effect to build the logarithm of amplitude vs. time function, named LPDT curve. The curves have an exponential growth shape, with an initial increase and a final plateau level. By analyzing and modelling the LPDT curves, the information about earthquake rupture process and earthquake magnitude can be obtained. We applied this method to the Chinese strong motion data from 2007 to 2015 with M_s ranging between 4 and 8. We used a refined model to reproduce the shape of the curves and different source models based on magnitude to infer the source-related parameters for the study dataset. Our study shows that the plateau level of LPDT curves has a clear scaling with magnitude, with no saturation effect for large events. By assuming a rupture velocity of 0.9 V_s , we found a consistent self-similar, constant stress drop scaling law for earthquakes in China with stress drop mainly distributed at a lower level (0.2 MPa) and a higher level (3.7 MPa). The derived relation between the magnitude and rupture length may be feasible for real-time applications of Earthquake Early Warning systems.

Keywords: P-wave amplitude parameter, magnitude, rupture length, stress drop, earthquake early warning

INTRODUCTION

The characterization of the seismic source in terms of earthquake magnitude and source radius (or length of the rupture) is now a routinely operation in any standard seismological laboratory. However, both parameters are generally computed off-line, through fairly complex procedures, mainly performed in the frequency domain. The seismic moment, for example, is estimated from the low frequency amplitude of displacement spectra. The source radius is typically obtained from the spectral corner frequency (Brune, 1970; Madariaga, 1976) or from time-domain, source duration measurements, generally available several minutes after the earthquake occurrence (Boatwright,

1980; Duputel et al., 2012). Although the fitting of spectral shapes is a straightforward operation, a major issue is the adequate correction of the observed spectra for path attenuation and site response effects.

In the context of Earthquake Early Warning (EEW), the point source characterization is usually based on the measurement of a few parameters (typically peak amplitude and/or characteristic period) in the early portion of the recorded P waves (3–4 s). These parameters are related to the earthquake size or to the peak ground shaking through empirical relationships (Allen and Kanamori, 2003; Kanamori, 2005; Wu and Zhao, 2006; Zollo et al., 2006; Böse et al., 2007; Wu and Kanamori, 2008; Zollo et al., 2010).

More recently, new strategies have been proposed to improve the accuracy of source parameter estimation for EEW applications and provide an estimate of the rupture area extent and the slip distribution on the fault. Among these strategies, some of them are based on the rapid inversion of geodetic and/or accelerometer data or fitting the spectrum in real-time (Allen and Ziv, 2011; Ohta et al., 2011; Colombelli et al., 2013; Caprio et al., 2011; Ziv and Lior, 2016). However, the rapid inversion of geodetic and/or accelerometer data need a catalog of the active faults for the construction of a rupture model plane in real-time (Colombelli et al., 2013). The azimuth dependency and the simplifying assumptions (e.g., directivity and segmentation) may introduce large discrepancies between modeled and observed spectra, leading to large variability in corner frequency estimates during the real-time spectrum inversion method (Ziv and Lior, 2016).

A second class of algorithms is based on the real-time spatial assessment of ground motion values. The FinDer algorithm (Böse et al., 2012), indeed, provides an estimate of the fault rupture extent and strike by continuously monitoring the spatial distribution of ground motions in real time. The results of this approach can be affected by the accuracy of near/far source classification and by the shortcomings in the GMPE used for the template generation (Böse et al., 2012, 2015).

More innovative approaches to EEW bypass the real-time source parameter estimation (location and magnitude) and use physics-based data assimilation techniques to directly predict the incoming evolution of ground shaking (PLUM) algorithm (Hoshiba and Aoki, 2015).

Recently, Colombelli and Zollo (2015) looked at the time evolution of the early P-wave information and used it as a proxy for the rupture process of earthquakes to extract the seismic moment and rupture extent of moderate-to-large Japanese earthquake records., Nazeri et al. (2019) explored a similar approach using strong-motion data of the 2016–2017 Central Italy sequence and estimated moment magnitude, fault length and average stress drop for each single event. The proposed method accounts for the effects of azimuth and distances by averaging the distance-corrected peak displacement among many stations, distributed over azimuth and distance, to approximate the moment rate function (MRF) and can be applied to general geometries with no need of prior knowledge of fault information. The proposed method is a remarkably simple and straightforward approach that does not

require any complex calculation for automatically estimating two main source parameters (the earthquake magnitude and the expected length of the rupture) before the rupture has finished.

Since 2005, the National Strong Motion Observation Network System of China was established. Stations in the network were mainly equipped with force balance accelerometers with a broadband frequency range of 0–80 Hz, which ensures that the network is reliable to record large quantities of high-quality strong-motion data for research purposes (Li et al., 2008).

Following the idea of Colombelli and Zollo (2015) and Nazeri et al. (2019), in this study we use a database of moderate-to-large Chinese earthquake records and explore a similar approach to estimate the earthquake magnitude and rupture length, and to provide an approximate estimate of the average stress drop to be used for Earthquake Early Warning and rapid response purposes. The aim is twofold: 1) establish source scaling relationships for moderate to large earthquakes in China and 2) build the foundation for further studying the feasibility of a network-based EEW method based on the time evolution of the early P-wave peak displacement amplitude.

DATA AND METHODOLOGY

Data Selection and Construction of LPDT Curves

For the present analysis, we selected the earthquakes occurred in China in the period 2007–2015. The magnitude of all the events (surface wave magnitude, M_s) varies between 4.0 and 8.0. To avoid the inclusion of bad quality data in our analysis, we selected seismic records with an epicentral distance smaller than 120 km, but for the M8 event we expanded the limit to 200 km and required that each event had at least three records. A total of 1293, 3-component accelerometric waveforms, relative to 88 earthquakes and 540 stations were used for the regression of P-wave peak displacement amplitude attenuation relationship, among which we selected 31 earthquakes (for a total of 617 records) with at least ten recording stations for the computation of the LPDT curve. **Figure 1A** shows the epicentral position of the selected earthquakes and the location of stations, in which two main seismic regions (Sichuan-Yunnan and Xinjiang regions) in China have been enlarged for clarity. **Figure 1B** shows the histogram distribution of the analysed records as a function of the epicentral distance and magnitude.

We identified the onset of the P wave on the vertical component of acceleration records, using a standard short-term/long-term average method for automatic picking (Allen, 1978). Then, we visually inspected all the available waveforms and made manual picks where necessary, to adjust potential mistakes from the automatic picking algorithm. After removing the mean value and the linear trend, the acceleration waveforms are integrated once to velocity and twice to get displacement. Finally, we applied a 0.075 Hz high-pass Butterworth filter to remove the low frequency drift on displacement records. We impose the zero-crossing of the signal amplitude at the onset of the P-wave, to eliminate any potential residual noise contaminations resulting from the double integration operation.

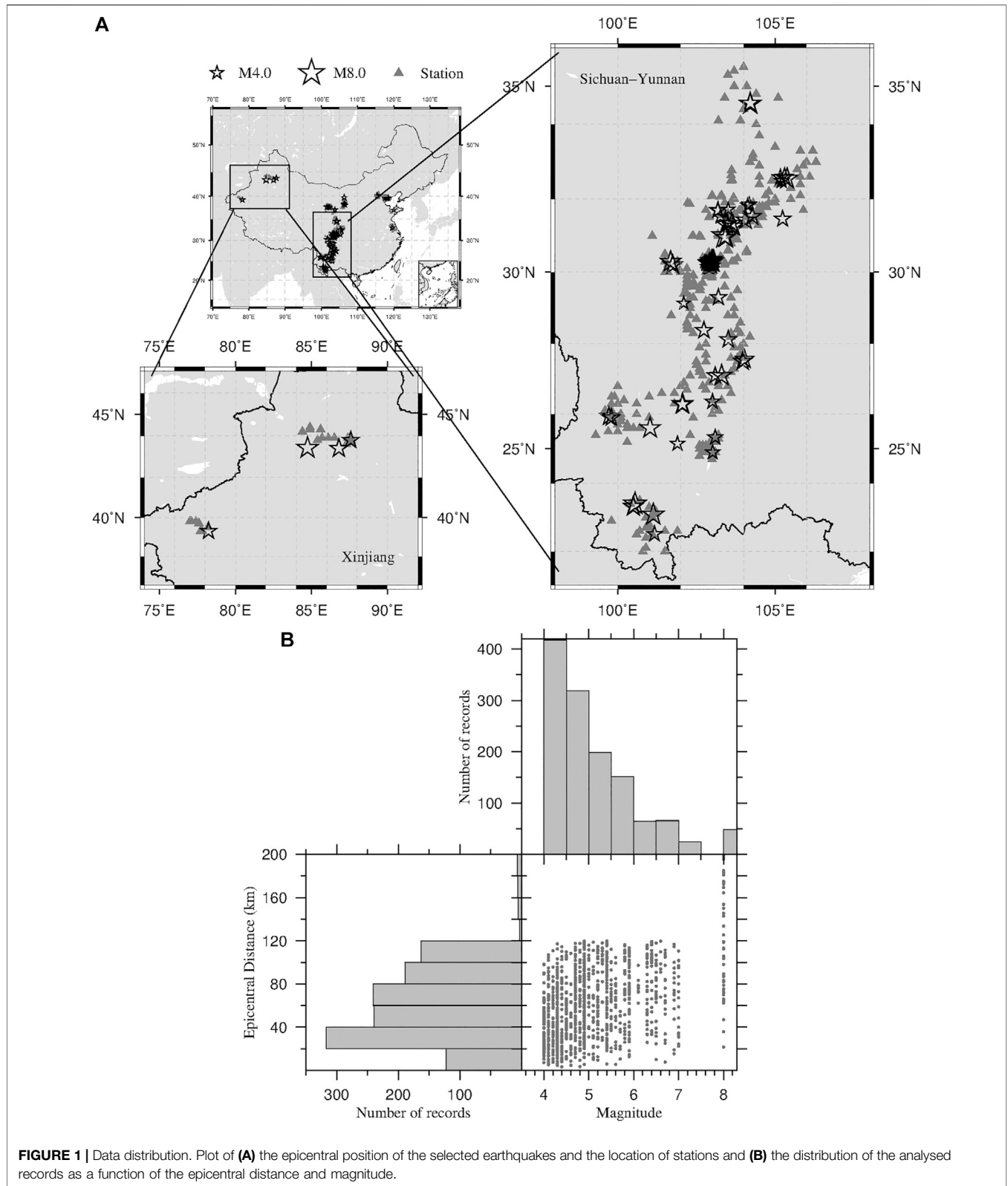
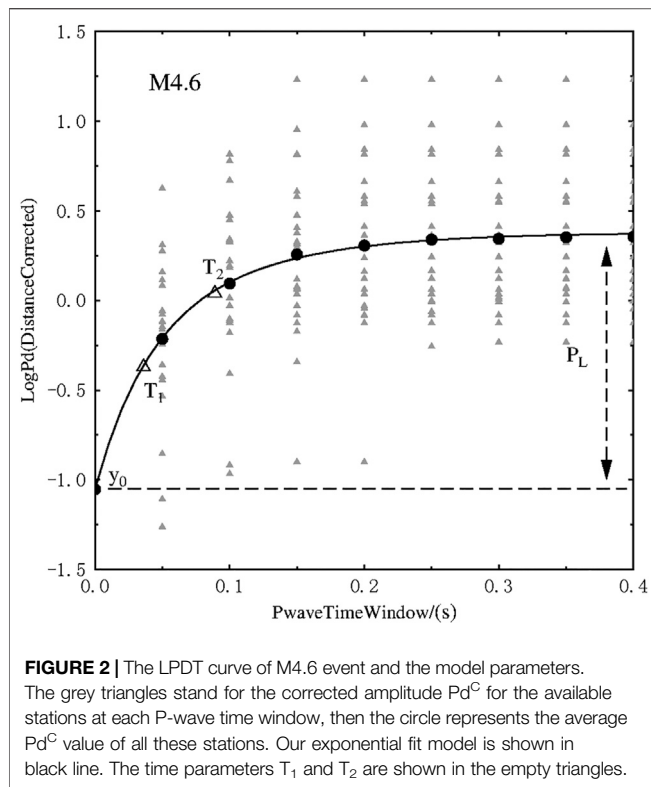


FIGURE 1 | Data distribution. Plot of **(A)** the epicentral position of the selected earthquakes and the location of stations and **(B)** the distribution of the analysed records as a function of the epicentral distance and magnitude.

We then measure the absolute maximum of the initial P-wave amplitude on the vertical component of displacement (named Pd) using an expanding time window, starting at the arrival of the

P-wave and moving forward with a time step of 0.01 s. The peak amplitude is related to the earthquake magnitude (M) and to the source-to-receiver distance (R) through an attenuation



relationship of the general form (Wu and Zhao, 2006; Zollo et al., 2006):

$$\log_{10}(Pd) = A + BM + C \log_{10}(R) \quad (1)$$

where Pd is the P-wave peak measurements and A , B and C are coefficients empirically determined from select dataset using 2 or 3 s after the P-wave arrival. Unlike the previous study, here we calibrated the coefficients by performing a specific least-squares multiple regression analysis, in which we fixed the distance attenuation coefficient (C) and chose a fixed length of the P-wave time window for the parameter measurements, which was set at 3 s for $M \leq 7$ and 9 s for $5.5 < M \leq 7$, respectively. Further details about the estimation of the coefficients of Eq. 1 are provided in **Supplementary Material**.

For the computation of the LPDT curve of each event, the peak amplitudes Pd of all records are measured at every P-wave time window and the distance-corrected amplitudes ($\log P^c d$) are obtained as $\log P^c d = \log Pd - C \log R$. In order to avoid the contamination by the S-waves on the selected portion of the P-wave, we picked out four stations with clear seismic phase randomly from the dataset in each distance bin (every 20 km). A total number of 40 records were used, and their S-wave arrival time were manually picked to estimate the coefficients of the following equation:

$$T_s - T_p = bR \quad (2)$$

where T_p is the P-wave onset time, T_s is the arrival time of the S-wave, R is the hypocentral distance in km, $b = 0.13$ is the

coefficient derived from a linear regression analysis. To minimize any potential S-wave contamination, we regarded $T_p + 0.8bR$ as the expected S-wave arrival. As the time window increases, the stations with the expected S-wave arrivals were automatically excluded to make sure only P-wave part involved in the computation. Finally, the LPDT curve is obtained by averaging the distance-corrected amplitude of all the valid stations at each time window. The computation of the curves stops when the number of stations is less than a minimum of data (Five stations).

Observation and Modelling of LPDT Curve

Figure 2 shows an example of the generated LPDT curve for the M4.6 event. The LPDT curve has an exponential growth shape with an initial increase, a gradual intermediate curvature and a final plateau level. Generally, the LPDT curve of larger event needs more time to reach the plateau and the plateau level of the curves scale with the final magnitude (**Figure 3A**).

The shape of the LPDT curve, as obtained from the average of many stations distributed over azimuth and distance, can be interpreted as a proxy of the Moment Rate Function (MRF), from the initial time up to its maximum peak value. Therefore, two essential features of the MRF, i.e., peak value and peak time, which are both related to the source properties, should be embodied in the LPDT curves. Following the idea of Colombelli and Zollo (2015), for near-triangular source time functions, the peak value of the MRF (related to the magnitude) will correspond to the plateau level of the LPDT curve, and the peak time of the MRF (related to rupture half-duration) is a proxy for the time at which the LPDT curve reaches its plateau level (Plateau Time). With this in mind, the magnitude and rupture duration can be estimated from the plateau level and the plateau time of the curves.

To model the LPDT curves, we fit data using the following function (Colombelli et al., 2020):

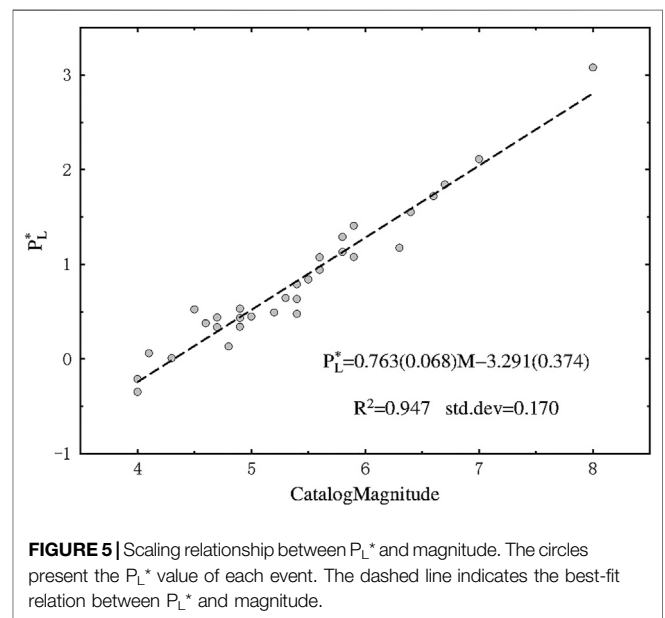
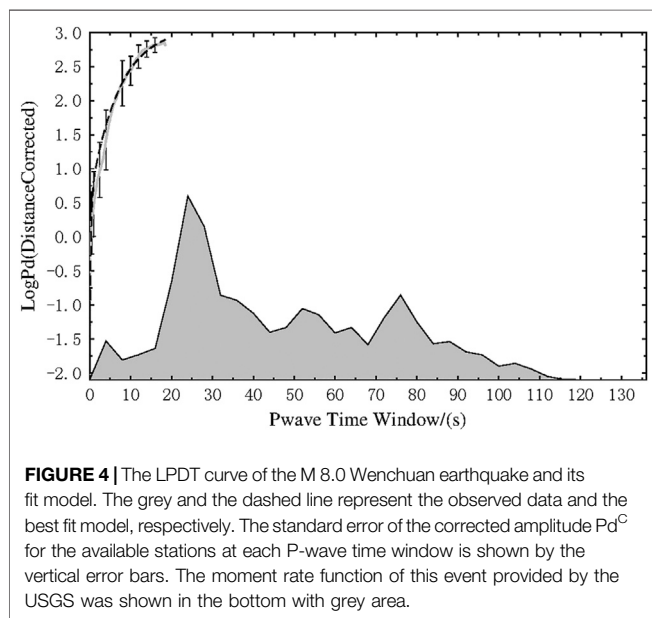
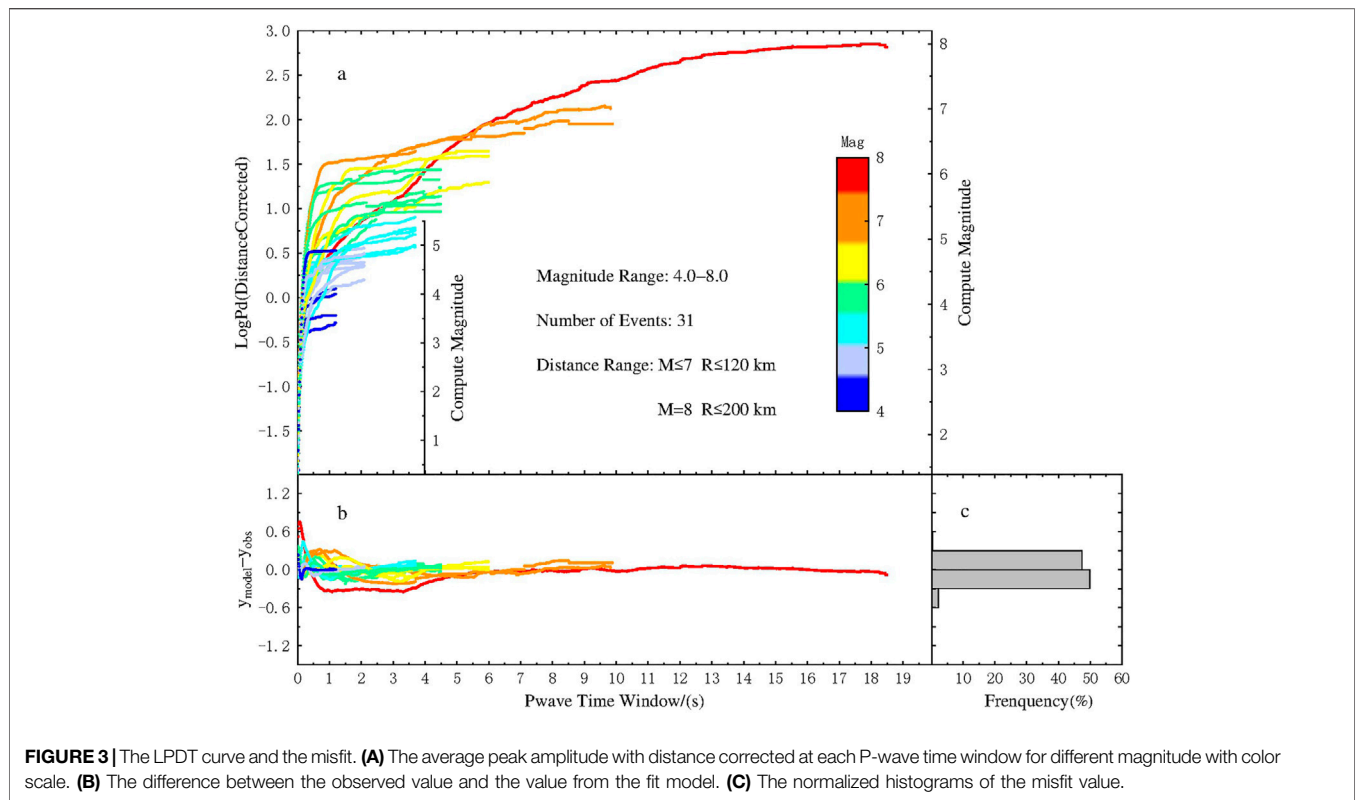
$$\log_{10} Pd(t) = P_L \left\{ 1 - \left[a e^{-\frac{t}{T_1}} + (1-a) \left(e^{-\frac{t}{T_2}} \right) \right] \right\} + y_0 \quad (3)$$

where y_0 is fixed as the first point of the curve, P_L is the interval between y_0 and the plateau level, a is the weighting factor which is set to 0.5, T_1 , and T_2 are the time parameters (here we define the larger value as T_2). T_1 controls the very initial part which usually has a faster increasing speed and T_2 represents the second part, whose increasing speed gradually becomes slower. This double corner time, exponential model accounts finely for the two different behaviors of LPDT curve—that is to say, a sharp increase to the plateau (ramp-like) for small events and a more gentle and smooth increase (exponential) for large events. The model parameters are shown in **Figure 2**.

We used a non-linear, weighted-fitting approach to model our curves, accounting for the standard error on each point of LPDT curves. Specifically, at each time step, the weight is obtained as:

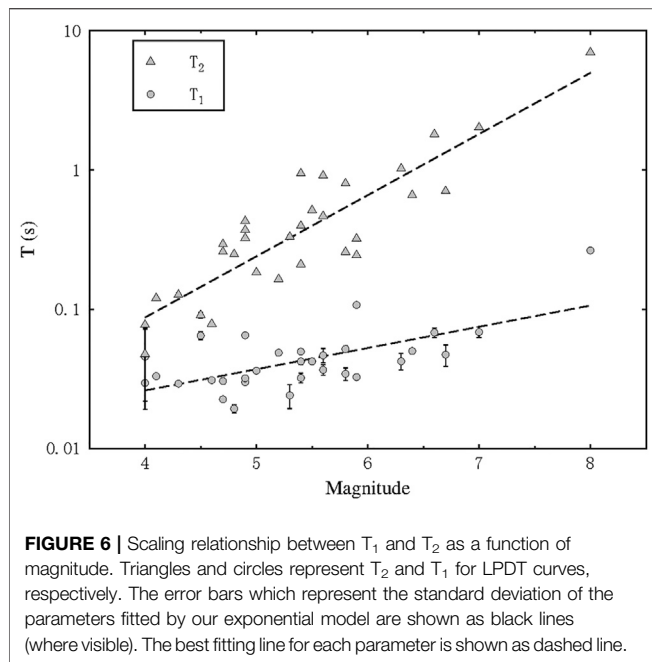
$$Weight = 1 / (N \cdot SE^2) \quad (4)$$

where SE is the standard error in each P-wave time window, N is the number of stations used for that time window. **Figure 3B** shows that the LPDT curves of all the events are quite well



reproduced by the fitting model, with an average residual of 0.3. Generally, at the beginning of the curve computation, several stations from a broad range of distances and azimuths are involved in the calculation, so that the scatter of data is large and the fitting procedure gives a smaller weight to this part, as compared to the plateau of the curves, which is instead, well

reproduced. A slightly larger (about 0.7) difference between the real data and the model is observed for the initial part of the curve of the M 8.0 Wenchuan earthquake, which could be related to the complexity of the source process of this peculiar event. Indeed, when looking at the seismic moment release of this event (**Figure 4**), a small peak value is observed at 4–5 s, before the



arrival of the absolute main peak value (at about 25 s), and this leads to a sag of the LPDT curve around 4 s.

RESULTS

We fit the LPDT curves with our exponential model and obtain the three relevant parameters mentioned above (T_1 , T_2 , P_L) while y_0 has been fixed to the first point amplitude. For simplicity, we defined a new variable called $P_L^* = P_L + y_0$ to represent the true plateau level of the LPDT curves. Both the amplitude parameter (P_L^*) and the two characteristic times (T_1 and T_2) scale with earthquake magnitude. **Figure 5** shows the plateau level P_L^* as a function of magnitude. A good correlation between P_L^* and magnitude (the correlation coefficient reaches 0.95) can be found. The parameters T_1 and T_2 extracted from our fitting model are shown in **Figure 6** as a function of magnitude. As the best fitting line indicates, both parameters linearly increase with magnitude (in logarithmic scale). Due to the very rapid initial increase of the curves, T_1 and T_2 are close to each other for small events, while they gradually separate when the magnitude becomes larger and the initial part of the curves increases gently.

Magnitude Estimation

Once the observed amplitude has been corrected for the distance effect, the LPDT value at each P-wave time window can be associated to a corresponding magnitude using the coefficients of **Eq. 1** (**Supplementary Table S1**). **Figure 3** shows the dynamic process of estimating magnitude for the LPDT curve. The y axis on the left stands for the distance corrected P_d , and the corresponding magnitude or estimated magnitude scale is shown on the right. The magnitude then can be estimated accurately based on the true plateau level of the LPDT curves and the coefficients of **Eq. 1** listed in **Supplementary Table S1**. As

shown in **Figure 3**, the occurrence of the plateau for large events ($M > 6-7$) needs more than 9 s after the P-wave arrival, suggesting that the typical approaches for the magnitude estimate using fixed 3–4 s P-wave time windows (PTWs) would provide underestimated magnitudes for such large events. Moreover, the B coefficient (calibrated using a 3 s PTW) could not be suitable to compute the corresponding magnitude based on the P_L^* obtained in a longer time window. We therefore choose two magnitude ranges, with two different PTW lengths, to calibrate and use the optimal coefficients (**Supplementary Table S1**) for magnitude estimation. In this way, when an event reached its plateau within 4 s, we use the relation coefficients A and B for fixed 3 s PTW, while we used the coefficients A and B established with a fixed 9 s PTW when its LPDT curve keeps increasing after 4 s.

The estimated final magnitude based on the P_L^* for the LPDT curve and obtained with the two sets of coefficients for small and large events respectively, is plotted in **Figure 7** as a function of the catalog magnitude. As it can be seen in **Figure 7**, most of the points are distributed around the dashed line representing the 1:1 relationship between the estimated magnitude and the catalog magnitude. The scatter of data is rather small, with an average estimated error of 0.23 magnitude units.

Prediction of Rupture Length and Estimation of Stress Drop $\Delta\sigma$

The rupture duration is the total duration of a seismic event, given by the whole-time length of the moment rate function (Vallée,

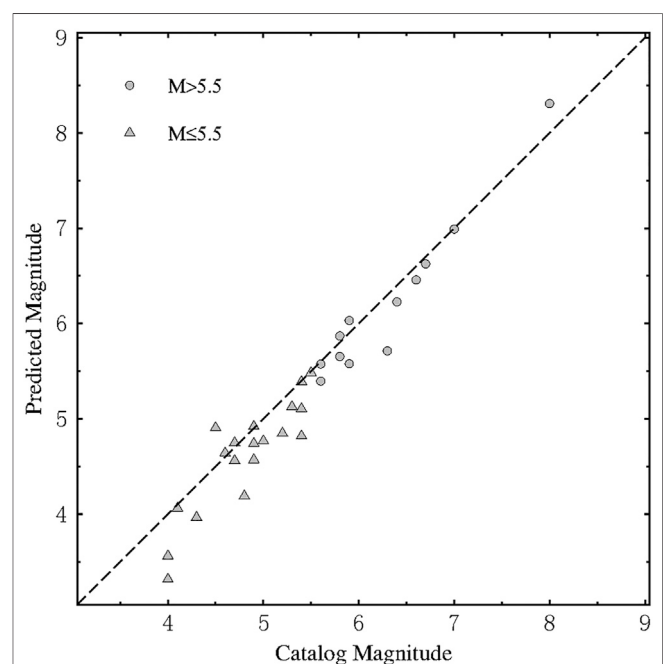


FIGURE 7 | The estimation of the magnitude and catalog magnitude. The dashed line corresponds to the 1:1 scaling. The triangles and circles indicate the estimated magnitude with P_L^* using the relation coefficients A and B for a fixed 3 s PTW and a fixed 9 s PTW, respectively.

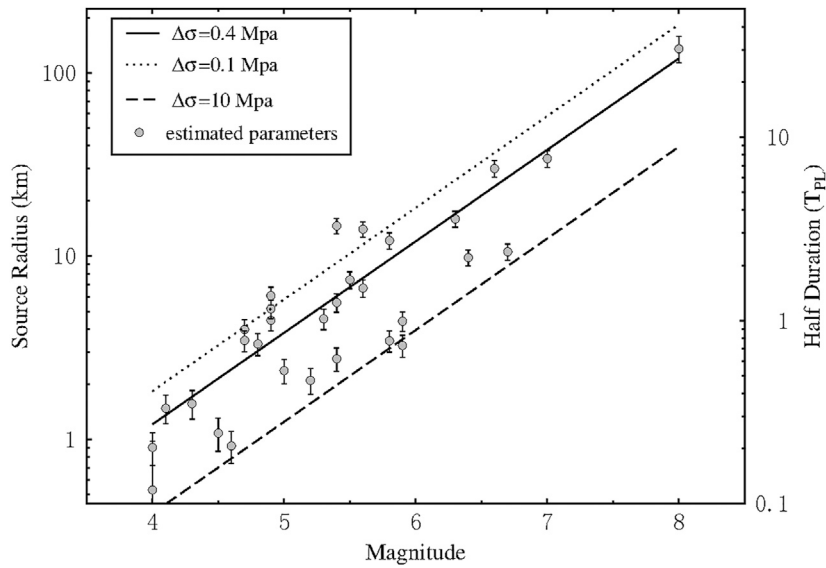


FIGURE 9 | The scaling relation between source radius and magnitude with a fixed rupture velocity of 0.9 Vs. The right y-axis represents the corresponding Half-duration. The circles stand for the T_{PL} parameter extracted from LPDT curve. The estimated errors computed through the error propagation theory are shown by the vertical error bars. The dotted line and dashed line represent the theoretical scaling with constant $\Delta\sigma = 0.1$ and 10 MPa, respectively. The averaged constant $\Delta\sigma$ of the analysed dataset are shown in the solid line.

and the source radius was given as follows (Aki and Richards, 2002):

$$T_{PL} = \langle HD \rangle = \frac{\int_0^{\frac{\pi}{2}} \frac{a}{V_r} \left(1 - \frac{V_r \sin\theta}{V_p}\right) d\theta}{\frac{\pi}{2}} = \frac{a}{V_r} \left(1 - \frac{2}{\pi} \frac{V_r}{V_p}\right) \quad (6)$$

where a is the source radius, V_r is rupture velocity, θ is the polar angle of the observation point and V_p is the P-wave velocity. Given the half-duration of the source, the source radius of the analysed events can be estimated.

Figure 9 shows the predicted source radius as a function of magnitude and its corresponding half-duration with a fixed rupture velocity of 0.9 Vs. Based on the computation of stress drop ($\Delta\sigma$) for the circular model using the source radius (a) and the seismic moment (M_0) (Keilis-Borok, 1959), $\Delta\sigma = \frac{7}{16} \frac{M_0}{a^3}$, the theoretical scaling lines of the source radius as a function of M with a constant $\Delta\sigma = 0.1$ and 10 MPa were given in the same figure as a comparison. The predicted source radius shows a similar increasing trend with the theoretical lines, indicating that the source radius of the analysed events has a consistent self-similar, constant stress drop scaling with magnitude. We fit the source radius with a weight-based fitting approach (same as Eq. 4, here, the SE is the standard error of the source radius computed from the predicted T_{PL} and its error obtained by the error propagation theory) to obtain the best-fit constant stress drop of 0.4 MPa. In addition, we repeated the process by setting $V_r = 0.7$ Vs and $V_r = 0.8$ Vs, and found that the mean value of $\Delta\sigma$ are 1.0 and 0.6 MPa, respectively.

The definition of rupture length changes in case of a circular fault (rupture length = rupture radius) and long-rectangular fault (rupture length = larger rectangular fault dimension). For a circular fault, the rupture lengths (source radius) predicted from LPDT curve were

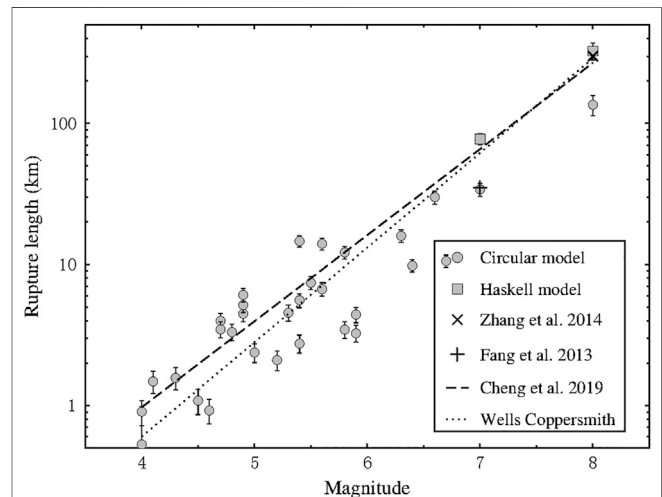
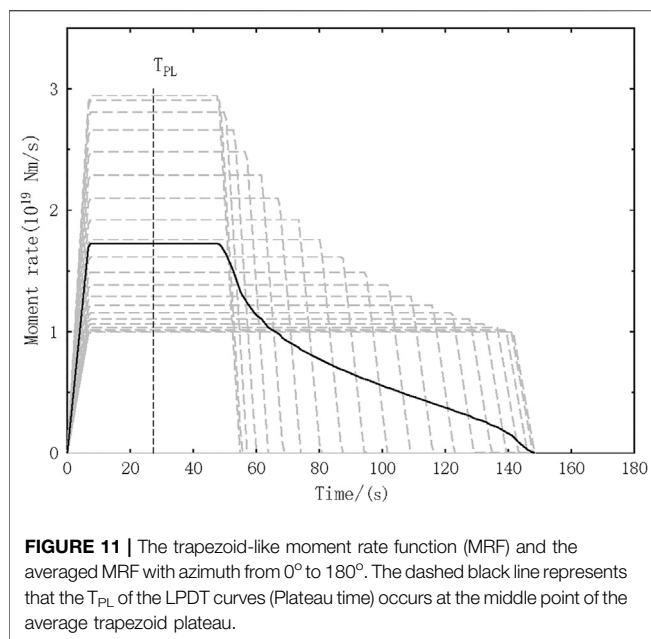


FIGURE 10 | The scaling relationship between the predicted rupture length and M . The circles and the squares are the predicted rupture length from circular model and Haskell model, respectively. The dashed line is the linear regression relationship in mainland China calibrated by Cheng et al. (2019). The dotted line represents the relationship proposed by Wells and Coppersmith (1994). The diagonal cross and cross are the results of M 8.0 Wenchuan earthquake by Zhang et al. (2014) and M 7.0 Lushan earthquake by Fang et al. (2013), respectively. The estimated errors computed through the error propagation theory are shown by the vertical error bars.

shown in **Figure 10**. As the figure indicates, most of our predicted rupture lengths as a function of magnitude agrees with the magnitude-rupture scaling relation studied by Cheng et al. (2019)



using 91 earthquakes in Mainland China and the empirical scaling relation for strike-slip earthquakes with M 4.8 to M 8.1 proposed by Wells and Coppersmith (1994). However, our predicted results were smaller than the rupture length of two models in the moderate-large magnitude range (M 7.0 Lushan earthquake and M 8.0 Wenchuan earthquake). To better assess the performances of our LPDT scheme in predicting rupture length, we collect the rupture lengths of these two largest events derived from other methodologies. Our approach provides a rupture length of 34 km for the M 7.0 Lushan earthquake, which is consistent with the results of relocated aftershocks by Fang et al. (2013) ($L \sim 35$ km) and the inversion results by Liu et al. (2013) ($L \sim 28$ km). For the M 8.0 Wenchuan earthquake, our predicted rupture length of 135 km is obviously underestimated as compared to the inversion results of Zhang et al. (2014) ($L \sim 300$ km) and the observed aftershock distribution over a length of 330 km (Huang et al., 2008).

The circular model is well suitable for small-to-moderate magnitudes (i.e., $M < 6$). Here, we also investigated the results of large magnitudes when applying the rectangular source model of Haskell. The far-field displacement radiated by a Haskell type fault model is equivalent to the convolution of two box-car functions of different amplitude and durations: rise time (τ) and rupture time (T_R). The resulting function has a trapezoidal shape with total duration given by the sum of $\tau + T_R$. The rupture time T_R depends on the finite length of the fault (L) and the azimuth (θ) between source and receiver (Haskell, 1964):

$$T_R = \frac{L}{V_r} \left(1 - \frac{V_r}{V_p} \cos\theta \right) \quad (7)$$

The rise time τ is independent of azimuth (Hwang et al., 2011) and can be obtained using the following relationship derived by Melgar and Hayes (2017) from a database of finite faults:

$$\log_{10}(\tau) = -5.323 + 0.293 \log_{10}(M_0) \quad (8)$$

Figure 11 shows an example of the average total duration of Haskell model with azimuth (θ) changed from 0° to 180°. Assuming that T_{PL} is the middle point of the average trapezoid plateau, the following relationship between L and T_{PL} can be obtained and be used for estimating rupture length of large events when assuming the Haskell model:

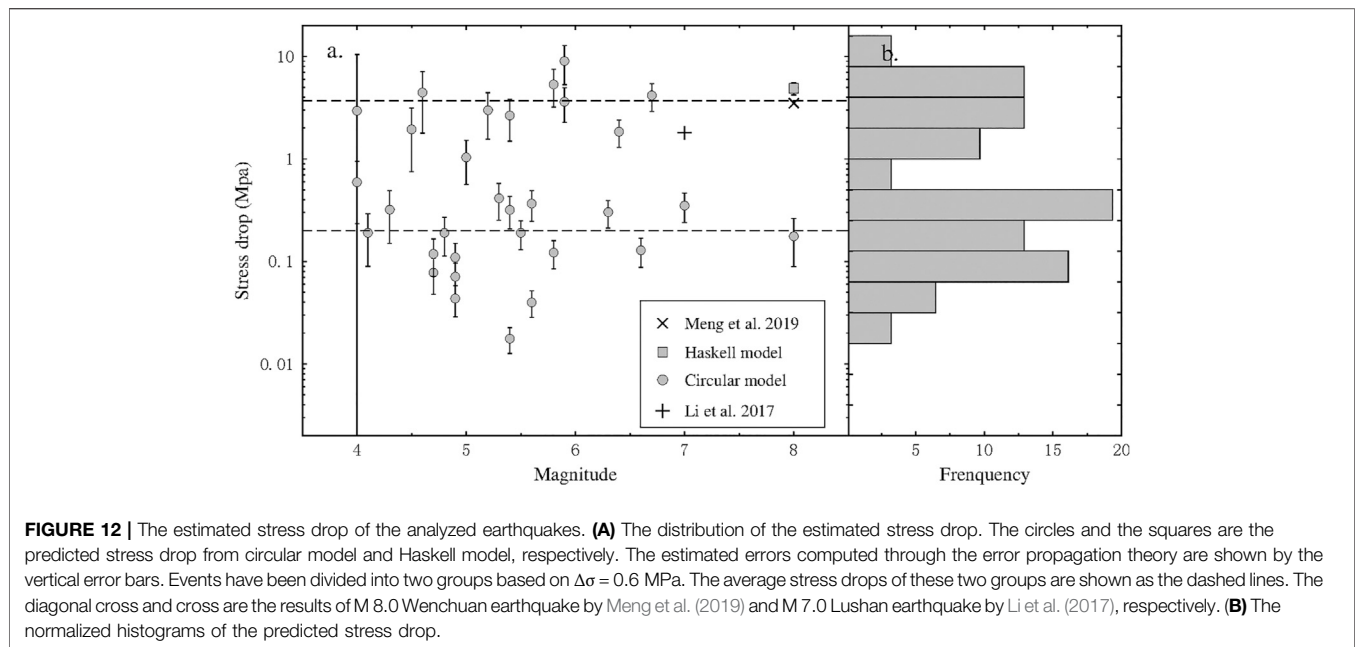
$$T_{PL} = \frac{1}{2} \left(\tau + \frac{L}{V_r} \left(1 - \frac{V_r}{V_p} \right) \right) \quad (9)$$

We computed the predicted rupture length for the two largest events using the Haskell model. As shown in **Figure 10**, with the same T_{PL} , applying the Haskell model appears to predict larger rupture lengths than the results using circular model. Specifically, we obtain an estimate of rupture length of 326 km without underestimation for Wenchuan earthquake, whereas the rupture length of Lushan earthquake has been overestimated ($L = 77.3$ km). The circular model produced a triangle-like MRF, as the Sato & Hirasawa moment rate Function of $M = 5$ event shown in the **Figure 8A** indicates, the peak time (T_{PL}) is almost half-duration. However, as the MRF of M 8.0 Wenchuan earthquake (download from USGS, shown in **Figure 4**) indicates, the MRF of some large events usually have the major peak occurring at the beginning of the rupture and followed by a long-time duration coda (Vallée, 2013). In this case, the circular model with a triangle-shape MRF may be not able to correctly reproduce this kind of source time function, and considering the peak time as the half-duration of the large events may result into underestimated rupture lengths. The averaged MRF from Haskell model shown in **Figure 11** reaches its peak (T_{PL}) around 1/5 of the total duration, which is more like the characteristic of MRF of the large magnitude earthquakes stated above. Moreover, for large earthquakes, the width (W) of the fault is already saturated, i.e., equal to the thickness of the brittle fracturing zone in the lithosphere. Accordingly, the growth of the fault area with increasing seismic moment (M_0) is in the length direction only (Bormann et al., 2009; Cheng et al., 2019). Therefore, in the situation of $L \gg W$ for large events, the Haskell model is more appropriate. Since the rupture surface of Lushan earthquake presents the focal characteristics of small-moderate earthquakes ($L \approx W$) (Chen et al., 2013; Hao et al., 2013), the Haskell model is not suitable for this event leading to an overestimated rupture length.

According to the derived rupture length of the analysed events, the stress drop can be computed based on different geometrical faults. Madariaga (1977) proposed that the general form $\Delta\sigma = \frac{M_0}{CSW} \approx \frac{M_0}{CS^{3/2}}$ (S is the rupture surface), where $C = \frac{16}{7\pi}$ for a circular fault, same as Keilis-Borok (1959)'s formula $\Delta\sigma = \frac{7}{16} \frac{M_0}{a^3}$ and $C = \frac{\pi}{2}$ for a long rectangular fault ($L \gg W$) as follows:

$$\Delta\sigma = \frac{2}{\pi} \frac{M_0}{W^2 L} \quad (10)$$

where W is the rupture width. Referring to the observation of Cheng et al. (2019) that large events with $M > 6.7$ have a nearly constant rupture width of ~ 20 km, here, we set W to 20 km.



We therefore suggest to use the circular model for small-moderate-strong events ($M \leq 7$) and the Haskell model (rectangle model) for large events ($M > 7$) in the estimation of rupture length and stress drop. The computed stress drop of each event is shown in **Figure 12**. After applying the rectangle source model for M 8.0 Wenchuan earthquake, the derived stress drop = 4.9 MPa is comparable with the results of Meng et al. (2019) (3.5 MPa). However, the circular model in this study provides an underestimated stress drop of 0.4 MPa for M 7.0 Lushan earthquake when comparing with the results (1.8 MPa) obtained by Li et al. (2017). As **Figure 12B** shows, the stress drops vary from 0.01 to 10 MPa. We divide the events into two groups based on $\Delta\sigma = 0.6$ MPa and calculate the averaged stress drop for these two groups. The higher stress drop group ($\Delta\sigma > 0.6$ MPa) has an averaged stress drop of 3.7 MPa, which is close to the world-wide measured median value of 4 MPa (Allmann and Shearer, 2009). The lower stress drop group with an averaged stress drop of 0.2 MPa consists of 19 events, in which half of the events are the aftershocks of the M 8.0 Wenchuan earthquake and the M 7.0 Lushan earthquake. Consistent with Wang et al. (2018), the lower stress drop of aftershocks may result from the remaining locked parts on the fault plane of the mainshock. All these source parameters of the analyzed events ($M \geq 5.5$) are summarized in **Table 1**.

DISCUSSION AND CONCLUSION

In this study, we generalized the approach proposed by Colombelli and Zollo (2015) to estimate the source parameters of a set of Chinese earthquakes with magnitude ranging from 4 to 8. The methodology is based on the use of the time evolution of the P wave (LPDT curve) as a proxy for the source time function to extract earthquake magnitude and rupture duration.

Comparing with the previous works by Colombelli and Zollo (2015) and Nazeri et al. (2019), we used the double corner time, exponential model proposed by Colombelli et al. (2020) for better modeling the behavior of LPDT curves. We improved the magnitude estimation based on the plateau level of LPDT curve, by using two different scaling coefficients with fixed C, which have been properly calibrated. Based on the analysis of 31 events in the magnitude range between 4 and 8, we found that the plateau level of LPDT curves has a strong correlation with magnitude (the coefficient of correlation is up to 0.95). Comparing with the catalog magnitude of the analyzed events, our predicted magnitude from the displacement data shows an average deviation of 0.23 magnitude units. The time at which these estimates are available implicitly depends on the event itself. Small events have a rapid initial increase and reach the plateau quickly, and for these events, the magnitude estimates would be available within a short time from the first P-wave detection. For the large events, like Wenchuan earthquake (M 8.0), the time needed to reach the plateau is longer. The near-source stations with a short fraction portion of the P-wave time-series cannot provide robust magnitude estimates for these large events, which is consistent with our observation that the LPDT curve at this stage is still growing and the plateau has not yet been reached. However, the expansion of hypocentral distance allows to capture longer P-wave signal portion of large events, and thus we provide a magnitude estimation of 8.3 for the Wenchuan earthquake after the LPDT curve reaches its plateau. By capturing the curve that reaches its plateau or looking at larger distances, our approach can estimate the magnitude of large events accurately, without saturation effects, typically observed when using shorter P-wave time windows (Lomax and Michelini, 2009; Bormann and Saul, 2009; Colombelli et al., 2012).

Together with the plateau level, the plateau time (T_{PL}) of the LPDT curve has also a clear scaling with magnitude, being

TABLE 1 | List of source parameters including catalog magnitude (M_S), predicted magnitude (M_S^{PRED}), half duration, Rupture length (RL) and stress drop ($\Delta\sigma$) determined in this study for moderate-larger events ($M \geq 5.5$).

No	Location	Date	Epicenter		Magnitude			Half duration		Rupture parameters			References
			Lat.	Long.	M_S	M_S^{PRED}	M_W (source)	LPDT	GCMT	RL (km)	RL (WC94)	SSD (MPa)	
1	Wenchuan	2008/ 05/12	31.00	103.40	8.0	8.3	7.9 (GCMT)	30.4	21.8	135.5 (circular) 326 (Haskell) 300	290	0.2 4.9	This study Zhang, wang, zschau, et al. (2014) Huang et al., 2008 Meng et al., (2019)
2	Wenchuan (aftershock)	2008/ 05/13	31.43	104.06	5.8	5.9	5.6 (GCMT)	0.8	1.6	3.4 (circular) 4.3	9.7	5.3 0.7	This study Wang et al., (2018)
3	Wenchuan (aftershock)	2008/ 05/14	31.34	103.63	5.8	5.7	5.4 (GCMT)	2.7	1.3	12.2 (circular) 7.5	9.7	0.1 0.2	This study Wang et al., (2018)
4	Yaoan	2009/ 07/09	25.60	101.03	6.3	5.7	5.7 (GCMT)	3.6	1.8	16 (circular)	21.0	0.3	This study
5	Yiliang	2012/ 09/07	27.56	104.03	5.6	5.6	5.3 (GCMT)	3.1	1.1	14 (circular)	7.1	0.04	This study
6	Eryuan	2013/ 03/03	25.93	99.72	5.5	5.3	5.4 (GCMT)	1.7	1.2	7.4 (circular)	6.1	0.2	This study
7	Changji	2013/ 03/29	43.40	86.80	5.6	5.4	5.4 (GCMT)	1.5	1.3	6.7 (circular)	7.1	0.4	This study
8	Lushan	2013/ 04/20	30.30	103.00	7	7.0	6.6 (GCMT)	7.6	4.9	34 (circular) 77.3 (Haskell) 35 28	61.9	0.4 0.7	This study Fang et al., (2013) Liu et al., (2013) Li et al., (2017)
9	Minxian	2013/ 07/22	34.54	104.21	6.7	6.6	6.0 (GCMT)	2.4	2.4	10.6 (circular)	38.9	4.2	This study
10	Ludian	2014/ 08/03	27.11	103.33	6.6	6.5	6.2 (GCMT)	6.7	2.9	30.0 (circular) 12	33.4	0.1	This study Cheng et al., (2015)
11	Kangding	2014/ 11/22	30.29	101.68	6.4	6.2	6.1 (GCMT)	2.2	2.8	9.8 (circular) 20 16	24.5	1.9	This study Fang et al., (2015) Jiang et al., (2015)
12	Kangding	2014/ 11/25	30.20	101.75	5.9	5.6	5.7 (GCMT)	0.7	1.8	3.2 (circular)	11.3	9.0	This study
13	Jinggu	2014/ 12/06	23.32	100.50	5.9	6.0	5.5 (GCMT)	1.0	1.5	4.4 (circular)	11.3	3.6	This study

M_S^{PRED} = predicted ms, RL = rupture length = source radius (circular model), WC94 = Wells and Coppersmith (1994), SSD = static stress drop, GCMT data are available at www.globalcmt.org (last accessed May. 6, 2020).

approximately related to the half-duration of the source. In order to estimate the plateau time, we performed a series of simulations based on the Sato and Hirasawa (1973) circular rupture model and on the assumption that T_{PL} corresponds to the peak time of the MRF. We generated a set of MRFs exploring $\Delta\sigma$ and V_r values and studied the relation between T_{PL} and the time characteristic parameter T_2 . Finally, we established a linear scaling relationship between the two parameters for predicting the T_{PL} .

Considering the circular model with a symmetric triangular-shaped MRF, the obtained T_{PL} can be regarded as the Half-Duration (HD) of the events to predict the source radius. The obtained source radius in this study shows a consistent self-similar, constant stress drop scaling with magnitude. We obtained the best-fit stress drop (0.4 MPa) for the 31 analysed events, with fixing rupture velocity to 0.9 Vs. This value is lower than world-wide measured median value of 4 MPa (Allmann and Shearer, 2009), but it is comparable with the mean value of 0.5 MPa by studying the

strong-motion recordings of the Wenchuan aftershocks (2008–2013) (Wang et al., 2018).

One major result of this paper concerns the determination of the scaling law of earthquakes in China. We obtained the rupture length of the analysed events using circular model and found the M 8.0 Wenchuan earthquake has a shorter predicted rupture length with comparing to other results. We realize that for the largest events in the sequence, the circular fault model may underestimate the total rupture length. Thus, we suggested to estimate the rupture length of the large events ($M > 7$) assuming the Haskell, rectangular fault model. Our predicted rupture length of different source models as a function of M is close to the rupture scaling relationship proposed by Cheng et al. (2019) and Wells and Coppersmith (1994).

The most critical issue of the proposed methodology is to assume a triangular shape to represent the source function. The assumption of a circular fault model can be inadequate to describe the complexity of the source for large events, for which multiple

peaks of moment release can occur. Moreover, the rupture process of an earthquake is a chaotic process, and the simple exponential LPDT curve may hardly represent the complex nature of this process, especially at the very beginning. However, the now massive and well documented observation of LPDT empirical curves analysed in many worldwide seismic regions and in a wide magnitude and distance range confirm that the general ramp-like behavior of the curves is a universal evidence (Colombelli et al., 2012; Colombelli et al., 2015; Colombelli et al., 2020; Melgar et al., 2015; Trugman et al., 2019) which is well matched by the chosen exponential model (Colombelli et al., 2020). When the curve has reached its peak, the schematic representation with two parameters (plateau time and amplitude), may properly catch the essential features of the process we are interested in.

Concerning the anelastic attenuation effect on LPDT curves, the overall features of the curves are essentially dominated by the event magnitude, which mainly controls the plateau level and the time to reach this plateau, for each curve. Using similar LPDT curves, Colombelli et al., (2020) recently investigated the effect of anelastic attenuation on the shape of the curves. This was done both theoretically and through a careful and detailed analysis of real earthquake data. They found that the chosen anelastic attenuation parametrization (Eq. 1) is appropriate to correct the distance attenuation effect on LPDT curves and this does not produce a systematic effect on plateau and T_{PL} parameter determination in all the observed curves in the same distance range.

The source parameters of the larger events are a major focus of - and motivation for - the proposed methodology. Although the selected dataset has a relatively wide magnitude range from 4.0 to 8.0, there is an obvious lack of large-magnitude data for events with magnitudes between 7 and 8. The proposed methodology would be better verified through the application to other seismic areas, once that the proper calibration of scaling coefficients has been done. It is worth to mention that the findings (e.g., rupture scaling relation and stress drop distribution) obtained through applying the methodology to the selected events (31 earthquakes) are mainly based on the data from Sichuan-Yunnan region, and may not be applicable to other areas as they are.

We notice that in the presence of a jump in the increasing shape of the LPDT curve, our approach likely fits the curve with a longer T_2 thus resulting in a lower stress drop value. **Supplementary Figure S2** shows the LPDT curve for the M 6.6 Ludian earthquake: a jump in the curve is clearly visible around 3.5 s. A similar magnitude event (M 6.4) which has a normal LPDT curve shape without jumps is selected for comparison. Our double corner time, exponential model (Eq. 3) fits the LPDT curve of this M 6.4 event with a $T_2 = 0.66$ s. However, due to the presence of jump, our exponential model tends to find a parameter (T_1 and T_2) with slower growth to fit the middle part (2 ~ 4 s) of the LPDT curve for M 6.6 Ludian earthquake. This resulted in our model fitting the LPDT curve with a longer $T_2 = 1.8$ s. We further justify the effect of LPDT curve shape on the exponential fitting model in **Supplementary Figure S3**. The virtual LPDT curve with

normal LPDT curve shape was generated as follow: the initial increasing part (0 ~ 1.85 s) and the approach plateau part (4.26 ~ 6 s) are the same as the observed LPDT curve, and only the middle part, we add points with exponential growth. After using our exponential model to fit the curves separately, we obtained a $T_2 = 1.46$ s for the virtual LPDT curve with a normal shape and a slightly longer T_2 (1.8 s) for the observed LPDT curve with a jump in the middle. Thus, based on the relationship between T_2 and T_{PL} , the predicted T_{PL} (plateau time) of LPDT curve with normal shape then will be 5.3 s, whereas the T_{PL} of the LPDT curve with jump will be 6.7 s. The jumps on the curve can be given by different effects, both related to the source process itself, such as multiple peaks on the Moment Rate Function, and/or to propagation effects, such as the arrival of intermediate phases (preceding the S-wave arrival), arriving at a receiver within the coda of P-wave phase. However, the presence of jumps on the LPDT curves is not frequently observed in our catalogue, only happens in two events. Meanwhile, the jump in the LPDT curve does not have a serious impact on the derived parameters. Thus, we believe that, on average, this is a negligible effect on the overall estimation of rupture length and stress drop.

The shape of the curves may change in real-time, when we do not have all the available stations. As a perspective of the work, we could evaluate the feasibility of application in real-time, that can be relevant for EEW applications. The accurate estimation of the rupture extent and magnitude at the early stage of the process can be a useful piece of information to add to the early shake-map computation, and the estimation of ground shaking can be strongly improved by considering the effect of the finite fault (Colombelli et al., 2013). While in this off-line study we used the post-earthquake location instead of the real-time estimation, a reliable estimation of the earthquake location is needed for the real-time application. Having in mind that the far-field stations must wait enough time to reach the plateau of the curve for large events, we need more time to get the plateau information. Hence, the real-time application performance and the timeliness based on the network distribution for this approach will be further studied. A possible method could be that we can estimate the final curve at each time step with a given probability and study the real-time curve reached how many percent of the final curve (maybe after T_2) can give a reliable probability for estimating final curve.

DATA AVAILABILITY STATEMENT

The original contributions presented in the study are included in the article/**Supplementary Material**, further inquiries can be directed to the corresponding authors.

AUTHOR CONTRIBUTIONS

YW applied the methodology and drafted the manuscript; SC and AZ critically revised the paper and supervised the study; JS and SL provided suggestions on the results. All authors contributed to the article and approved the submitted version.

FUNDING

This research was financially supported by the National Key Research and Development Program of China (2018YFC1504003) and its provincial funding, the Italian Ministry of Research and the University of Naples Federico II (Project Number AIM1834927-3; E66C19000090001), and the Scientific Research Fund of Institute of Engineering Mechanics, China Earthquake Administration (2016A03).

ACKNOWLEDGMENTS

We thank the China Strong Motion Network Centre (CSMNC) at the Institute of Engineering Mechanics, China Earthquake Administration, for providing the ground motion recording data. We would like to thank the University of Naples Federico II where the work has been

REFERENCES

- Aki, K., and Richards, P. G. (2002). *Quantitative seismology*. Sausalito, CA: University Science Books.
- Allen, R. M., and Kanamori, H. (2003). The potential for earthquake early warning in southern California. *Science* 300 (5620), 786–789. doi:10.1126/science.1080912
- Allen, R. M., and Ziv, A. (2011). Application of real-time GPS to earthquake early warning. *Geophys. Res. Lett.* 38 (16) doi:10.1029/2011gl047947
- Allen, R. V. (1978). Automatic earthquake recognition and timing from single traces. *Bull. Seismological Soc. America* 68 (5), 1521–1532.
- Allmann, B. P., and Shearer, P. M. (2009). Global variations of stress drop for moderate to large earthquakes. *J. Geophys. Res.* 114 (B1). doi:10.1029/2008jb005821
- Bilek, S. L., Lay, T., and Ruff, L. J. (2004). Radiated seismic energy and earthquake source duration variations from teleseismic source time functions for shallow subduction zone thrust earthquakes. *J. Geophys. Res.* 109 (B9), a. doi:10.1029/2004jb003039
- Brune, J. N. (1970). Tectonic stress and the spectra of seismic shear waves from earthquakes. *J. Geophys. Res.* 75 (26), 4997–5009. doi:10.1029/JB075i026p04997
- Boatwright, J. (1980). A spectral theory for circular seismic sources; simple estimates of source dimension, dynamic stress drop, and radiated seismic energy. *Bull. Seismological Soc. America* 70 (1), 1–27.
- Bormann, P., Baumbach, M., Bock, G., Grosser, H., Choy, G. L., and Boatwright, J. (2009). “Seismic sources and source parameters,” in *New manual of seismological observatory practice (NMSOP)*. Editor P. Bormann (Potsdam: Deutsches GeoForschungsZentrum GFZ), 1–94.
- Bormann, P., and Saul, J. (2009). “Earthquake magnitude,” in *Encyclopedia of complexity and systems science*. Editor R. Meyers (New York, N Y: Springer). doi:10.1007/978-0-387-30440-3_151
- Keilis-Borok, V. (1959). On estimation of the displacement in an earthquake source and of source dimensions. *Ann. Geofis. (Rome)* 12, 205–214. doi:10.4401/ag-5718
- Böse, M., Felizardo, C., and Heaton, T. H. (2015). Finite-fault rupture detector (FinDer): going real-time in Californian ShakeAlert Warning system. *Seismological Res. Lett.* 86 (6), 1692–1704. doi:10.1785/0220150154
- Böse, M., Heaton, T. H., and Hauksson, E. (2012). Real-time finite fault rupture detector (FinDer) for large earthquakes. *Geophys. J. Int.* 191 (2), 803–812. doi:10.1111/j.1365-246X.2012.05657.x
- Böse, M., Ionescu, C., and Wenzel, F. (2007). Earthquake early warning for Bucharest, Romania: novel and revised scaling relations. *Geophys. Res. Lett.* 34 (7). doi:10.1029/2007gl029396
- Caprio, M., Lancieri, M., Cua, G. B., Zollo, A., and Wiemer, S. (2011). An evolutionary approach to real-time moment magnitude estimation via inversion of displacement spectra. *Geophys. Res. Lett.* 38 (2), a. doi:10.1029/2010gl045403

carried out during the visiting period. We would also like to thank Jia Cheng (Institute of Crustal Dynamics, China Earthquake Administration) for the discussion about the calculation of stress drop. The moment rate function of the M 8.0 Wenchuan earthquake has been provided by the USGS: <https://earthquake.usgs.gov/earthquakes/eventpage/usp000g650/finite-fault> (last accessed May 2020). This manuscript has been posted on Earth and Space Science Open Archive (ESSOAr) with a preprint service (<https://www.essoar.org/doi/abs/10.1002/essoar.10503831.1>).

SUPPLEMENTARY MATERIAL

The Supplementary Material for this article can be found online at: <https://www.frontiersin.org/articles/10.3389/feart.2021.616229/full#supplementary-material>.

- Chen, Y., Yang, Z., Zhang, Y., and Liu, C. (2013). From 2008 Wenchuan earthquake to 2013 Lushan earthquake (in Chinese). *Sci. China Ser. D: Earth Sci.* 43, 1064–1072.
- Cheng, J., Rong, Y., Magistrale, H., Chen, G., and Xu, X. (2019). Earthquake rupture scaling relations for mainland China. *Seismological Res. Lett.* 91 (1), 248–261. doi:10.1785/0220190129
- Cheng, J., Wu, Z., Liu, J., Jiang, C., Xu, X., Fang, L., et al. (2015). Preliminary report on the 3 august 2014, mw 6.2/ms 6.5 ludian, yunnan-sichuan border, southwest China, earthquake. *Seismological Res. Lett.* 86 (3), 750–763. doi:10.1785/0220140208
- Colombelli, S., Allen, R. M., and Zollo, A. (2013). Application of real-time GPS to earthquake early warning in subduction and strike-slip environments. *J. Geophys. Res. Solid Earth* 118 (7), 3448–3461. doi:10.1002/jgrb.50242
- Colombelli, S., Festa, G., and Zollo, A. (2020). Early rupture signals predict the final earthquake size. *Geophys. J. Int.* 223 (1), 692–706. doi:10.1093/gji/ggaa343
- Colombelli, S., and Zollo, A. (2015). Fast determination of earthquake magnitude and fault extent from real-time P-wave recordings. *Geophys. J. Int.* 202 (2), 1158–1163. doi:10.1093/gji/ggv217
- Colombelli, S., Zollo, A., Festa, G., and Kanamori, H. (2012). Early magnitude and potential damage zone estimates for the great Mw 9 Tohoku-Oki earthquake. *Geophys. Res. Lett.* 39 (22), a. doi:10.1029/2012gl053923
- Duputel, Z., Rivera, L., Kanamori, H., and Hayes, G. (2012). W phase source inversion for moderate to large earthquakes (1990–2010). *Geophys. J. Int.* 189 (2), 1125–1147. doi:10.1111/j.1365-246X.2012.05419.x
- Fang, L., Wu, J., Liu, J., Cheng, J., Jiang, C., Han, L., et al. (2015). Preliminary report on the 22 november 2014 Mw 6.1/ms 6.3 kangding earthquake, western sichuan, China. *Seismological Res. Lett.* 86 (6), 1603–1613. doi:10.1785/0220150006
- Fang, L., Wu, J., Wang, W., Lü, Z., Wang, C., Yang, T., et al. (2013). Relocation of the mainshock and aftershock sequences of M 5.7.0 Sichuan Lushan earthquake. *Chin. Sci. Bull.* 58 (28–29), 3451–3459. doi:10.1007/s11434-013-6000-2
- Hao, J., Ji, C., Wang, W., and Yao, Z. (2013). Rupture history of the 2013 Mw 6.6 Lushan earthquake constrained with local strong motion and teleseismic body and surface waves. *Geophys. Res. Lett.* 40 (20), 5371–5376. doi:10.1002/2013gl056876
- Haskell, N. A. (1964). Total energy and energy spectral density of elastic wave radiation from propagating faults. *Bull. Seismological Soc. America* 54 (6A), 1811–1841.
- Heaton, T. H. (1990). Evidence for and implications of self-healing pulses of slip in earthquake rupture. *Phys. Earth Planet. Interiors* 64 (1), 1–20. doi:10.1016/0031-9201(90)90002-f
- Hoshiba, M., and Aoki, S. (2015). Numerical shake prediction for earthquake early warning: data assimilation, real-time shake mapping, and simulation of wave propagation. *Bull. Seismological Soc. America* 105 (3), 1324–1338. doi:10.1785/0120140280

- Huang, Y., Wu, J., Zhang, T., and Zhang, D. (2008). Relocation of the M8.0 Wenchuan earthquake and its aftershock sequence. *Sci. China Ser. D-earth Sci.* 51 (12), 1703–1711. doi:10.1007/s11430-008-0135-z
- Hwang, R.-D., Chang, J.-P., Wang, C.-Y., Wu, J.-J., Kuo, C.-H., Tsai, Y.-W., et al. (2011). Rise time and source duration of the 2008 M 7.9 Wenchuan (China) earthquake as revealed by Rayleigh waves. *Earth Planet. Sp* 63 (5), 427–434. doi:10.5047/eps.2011.01.002
- Jiang, G., Wen, Y., Liu, Y., Xu, X., Fang, L., Chen, G., et al. (2015). Joint analysis of the 2014 Kangding, southwest China, earthquake sequence with seismicity relocation and InSAR inversion. *Geophys. Res. Lett.* 42 (9), 3273–3281. doi:10.1002/2015gl063750
- Kanamori, H. (2005). Real-time seismology and earthquake damage mitigation. *Annu. Rev. Earth Planet. Sci.* 33 (1), 195–214. doi:10.1146/annurev.earth.33.092203.122626
- Li, J., Liu, C., Zheng, Y., and Xiong, X. (2017). Rupture process of the M 7.0 Lushan earthquake determined by joint inversion of local static GPS records, strong motion data, and teleseismograms. *J. Earth Sci.* 28 (2), 404–410. doi:10.1007/s12583-017-0757-1
- Li, X., Zhou, Z., Yu, H., Wen, R., Lu, D., Huang, M., et al. (2008). Strong motion observations and recordings from the great Wenchuan Earthquake. *Earthq. Eng. Eng. Vib.* 7 (3), 235–246. doi:10.1007/s11803-008-0892-x
- Liu, C., Zheng, Y., Ge, C., Xiong, X., and Hsu, H. (2013). Rupture process of the M 7.0 Lushan earthquake, 2013. *Sci. China Earth Sci.* 56 (7), 1187–1192. doi:10.1007/s11430-013-4639-9
- Lomax, A., and Michelini, A. (2009). Mwpd: a duration-amplitude procedure for rapid determination of earthquake magnitude and tsunamigenic potential from P-waveforms. *Geophys. J. Int.* 176 (1), 200–214. doi:10.1111/j.1365-246X.2008.03974.x
- Madariaga, R. (1976). Dynamics of an expanding circular fault. *Bull. Seismological Soc. America* 66 (3), 639–666.
- Madariaga, R. (1977). Implications of stress-drop models of earthquakes for the inversion of stress drop from seismic observations. *Pageoph* 115, 301–316. doi:10.1007/bf01637111
- Melgar, D., Crowell, B. W., Geng, J., Allen, R. M., Bock, Y., Riquelme, S., et al. (2015). Earthquake magnitude calculation without saturation from the scaling of peak ground displacement. *Geophys. Res. Lett.* 42 (13), 5197–5205. doi:10.1002/2015gl064278
- Melgar, D., and Hayes, G. P. (2017). Systematic observations of the slip pulse properties of large earthquake ruptures. *Geophys. Res. Lett.* 44 (19), 9691–9698. doi:10.1002/2017gl074916
- Meng, L., Zang, Y., McGarr, A., and Zhou, L. (2019). High-frequency ground motion and source characteristics of the 2008 wenchuan and 2013 lushan, China, earthquakes. *Pure Appl. Geophys.* 177 (1), 81–93. doi:10.1007/s00024-019-02291-4
- Nazeri, S., Colombelli, S., and Zollo, A. (2019). Fast and accurate determination of earthquake moment, rupture length and stress release for the 2016–2017 Central Italy seismic sequence. *Geophys. J. Int.* 217 (2), 1425–1432. doi:10.1093/gji/ggz097
- Ohta, Y., Miura, S., Ohzono, M., Kita, S., Iinuma, T., Demachi, T., et al. (2011). Large intraslab earthquake (2011 April 7, M 7.1) after the 2011 off the Pacific coast of Tohoku Earthquake (M 9.0): coseismic fault model based on the dense GPS network data. *Earth Planet. Sp* 63 (12), 1207–1211. doi:10.5047/eps.2011.07.016
- Sato, T., and Hirasawa, T. (1973). Body wave spectra from propagating shear cracks. *J. Phys. Earth* 21 (4), 415–431. doi:10.4294/jpe1952.21.415
- Trugman, D. T., Page, M. T., Minson, S. E., and Cochran, E. S. (2019). Peak ground displacement saturates Exactly when expected: implications for earthquake early warning. *J. Geophys. Res. Solid Earth* 124 (5), 4642–4653. doi:10.1029/2018jb017093
- Vallée, M. (2013). Source time function properties indicate a strain drop independent of earthquake depth and magnitude. *Nat. Commun.* 4 (1), 2606. doi:10.1038/ncomms3606
- Wang, H., Ren, Y., and Wen, R. (2018). Source parameters, path attenuation and site effects from strong-motion recordings of the Wenchuan aftershocks (2008–2013) using a non-parametric generalized inversion technique. *Geophys. J. Int.* 212 (2), 872–890. doi:10.1093/gji/ggx447
- Wang, W., Wu, J., Fang, L., Lai, G., Yang, T., and Cai, Y. (2014). Swave velocity structure in southwest China from surface wave tomography and receiver functions. *J. Geophys. Res. Solid Earth* 119 (2), 1061–1078. doi:10.1002/2013jb010317
- Wells, D. L., and Coppersmith, K. J. (1994). New empirical relationships among magnitude, rupture length, rupture width, rupture area, and surface displacement. *Bull. Seismological Soc. America* 84 (4), 974–1002.
- Wu, Y.-M., and Kanamori, H. (2008). Exploring the feasibility of on-site earthquake early warning using close-in records of the 2007 Noto Hanto earthquake. *Earth Planet. Sp* 60 (2), 155–160. doi:10.1186/BF03352778
- Wu, Y.-M., and Zhao, L. (2006). Magnitude estimation using the first three seconds P-wave amplitude in earthquake early warning. *Geophys. Res. Lett.* 33 (16). doi:10.1029/2006gl026871
- Zhang, Y., Wang, R., Zschau, J., Chen, Y.-t., Parolai, S., and Dahm, T. (2014). Automatic imaging of earthquake rupture processes by iterative deconvolution and stacking of high-rate GPS and strong motion seismograms. *J. Geophys. Res. Solid Earth* 119 (7), 5633–5650. doi:10.1002/2013jb010469
- Ziv, A., and Lior, I. (2016). Real-time moment magnitude and stress drop with implications for real-time shaking prediction. *Bull. Seismological Soc. America* 106 (6), 2459–2468. doi:10.1785/0120160091
- Zollo, A., Amoroso, O., Lancieri, M., Wu, Y.-M., and Kanamori, H. (2010). A threshold-based earthquake early warning using dense accelerometer networks. *Geophys. J. Int.* 183 (2), 963–974. doi:10.1111/j.1365-246X.2010.04765.x
- Zollo, A., Lancieri, M., and Nielsen, S. (2006). Earthquake magnitude estimation from peak amplitudes of very early seismic signals on strong motion records. *Geophys. Res. Lett.* 33 (23). doi:10.1029/2006gl027795

Conflict of Interest: The authors declare that the research was conducted in the absence of any commercial or financial relationships that could be construed as a potential conflict of interest.

Copyright © 2021 Wang, Colombelli, Zollo, Song and Li. This is an open-access article distributed under the terms of the Creative Commons Attribution License (CC BY). The use, distribution or reproduction in other forums is permitted, provided the original author(s) and the copyright owner(s) are credited and that the original publication in this journal is cited, in accordance with accepted academic practice. No use, distribution or reproduction is permitted which does not comply with these terms.